**Swansea University
Prifysgol Abertawe**

**Cronfa
Setting Research Free**

Cronfa - Swansea University Open Access Repository

_____

This is an author produced version of a paper published in :
The International Journal of Advanced Manufacturing Technology

Cronfa URL for this paper:
http://cronfa.swan.ac.uk/Record/cronfa18363

_____

_____

Investigation into the Effect of process parameters on microstructural and physical properties of 316L stainless steel parts by selective laser melting.

J. A. Cherry, [a*], H. M. Davies[a], S. Mehmood[a], N.P. Lavery[a], S.G.R.Brown[a],

J. Sienz[1]

[a]Advanced Sustainable Manufacturing Technologies (ASTUTE), Digital Technium, College of Engineering, Swansea University, Singleton Park, Swansea SA2 8PP, UK

[*] Corresponding author: J.A.Cherry@Swansea.ac.uk, tel.: +44 1792 606883; fax: +44 1792 601111

Abstract:

Additive manufacturing by selective laser melting (SLM) was used to investigate the effect of laser energy density on 316L stainless steel properties. Point distance and exposure time were varied and their impact on porosity, surface finish, microstructure, density and hardness, was evaluated.

The surface roughness was primarily affected by point distance with increased point distance resulting in increased surface roughness, R_a, from 10 µm to 16 µm. Material hardness reached a maximum of 225 HV at 125 J/mm^3 and was related to the material porosity; with increased porosity leading to decreased material hardness. Different types of particle coalescence leading to convex surface features were observed (sometimes referred to as balling); from small-ball features at low laser energy density to a mixture of both small and large ball features at high laser energy density. Laser energy density was shown to affect total porosity. The minimum amount of porosity, 0.38%, was observed at an energy density of 104.52 J/mm^3.

1. Introduction

Additive layer manufacturing (ALM) by selective laser melting (SLM) is an advanced manufacturing process which uses lasers to melt metal powders, one layer at a time to produce final net-shape components from 3D CAD. The process is suitable to manufacture complex parts which cannot be manufactured using conventional processes such as casting or forging. The process has been successfully demonstrated [1] to manufacture 316L parts. Apart from the manufacturing flexibility of the SLM process which enables production of multi-functional products and in comparison to subtractive production processes, ALM also allows a low 'buy-to-fly' ratio, reducing raw material costs.

In the last two decades ALM techniques have been widely studied with the drive to make them part of mainstream manufacturing. Various ALM techniques and applications have been described well elsewhere by Paul and Baskaran [2]. SLM is one of the most commonly used ALM techniques and the process is a potential manufacturing route for, bio-medical parts [3], aero applications [4], cooling inserts for castings [5] and dental prostheses [6].

Currently poor surface quality and residual porosity, in 316L parts manufactured via the SLM route, prevent its use for applications where high strength and fatigue resistance are the key requirements. It is well understood that the mechanical properties of SLM parts, like traditionally manufactured parts, depend not only on the microstructure but also on any typically porous defects and their morphology - which are controlled by the initial processing parameters. Therefore understanding the effects of processing parameters on microstructural evolution in SLM has become the focus of recent investigations. Previous work on 316L parts by Kruth et al. [1] reported on the effect of processing parameters on microstructure and mechanical properties. The effect of laser sintering parameters on structure-property relationships for low carbon steel powder [7], iron based powder [8], Ni-Cr alloys [9], and Ni based Waspaloy [10, 11] have already been reported and highlighted that even minor changes in any processing parameters can have large effects on the final material properties, both physical and microstructural.

The flexibility of the ALM process allows various processing parameters to be modified to alter the resultant energy imparted into the build. These parameters include, for example, laser power, hatch spacing, point distance, focal diameter and exposure time.

Previous studies have identified the effect of continuous lasers on the effect of 316L properties. This study aims to identify the effect of a modulated laser system on the material properties of 316L. The present study aims to investigate the effect of laser energy by varying processing parameters, point distance and exposure time, on porosity, surface finish, microstructure, density and hardness in ALM 316L stainless steel cubes.

2. Experimental

2.1. Processing parameters and material specification

Metallic parts have been produced using the SLM process by the Renishaw AM250. The AM250 uses an Nd:YAG laser in Q-switched mode with a maximum power of 200 W and laser spot diameter 70 μm. There are a wide range of parameters that can be varied in order to change the part properties and include but are not limited to, material specific parameters, laser parameters, scan parameters and environmental parameters.

Simchi [12] has shown a dependency of densification in iron based powders on processing parameters such as: laser power, scan rate, layer thickness, and scan line spacing etc. Kruth et al. [1] have studied the effect of scan speed and scan spacing on microstructural properties in 316L stainless steel.

The physical and microstructural properties of the material will be greatly influenced by the energy input during the laser melting process and with this in mind, the laser exposure time and overlap (point distance) were investigated in the present study.

The material used in the current investigation was 316L stainless steel powder, size range 15 to 45 μm, manufactured via gas atomisation. The specification and actual composition (as supplied) of the alloy are shown in Table 1.

Table 1 Composition of 316L stainless steel powder

Grade 316L		Fe	C	Si	Mn	P	S	Cr	Ni	Mo	N	Cu	O
Wt%	**Min**	Bal	-	-	-	-	-	17.5	12.5	2.25	-	-	-
	Max		0.03	0.75	2	0.025	0.01	18	13	2.5	0.1	0.5	0.1
	Actual		0.019	0.67	1.45	0.019	0.006	17.9	12.7	2.36	0.06	0.2	0.022

A 3 by 3 test matrix of 10X10X10 mm^3 cubes was produced with varying laser exposure time and point distance, Table 2. The levels of point distance, the distance between successive laser hits, and exposure time, the time the laser remains at one point, were selected to ensure a solid component was created from the resulting energy input, Q (J/mm^3), Eq.1. Therefore, approximately 75 J/mm^3 either side of the standard machine manufacturer operational parameter levels for 316L steel were used. The standard settings give an approximate energy input of 125 J/mm^3.

$$Q = \frac{laser\ power\left(\frac{exposure\ time}{hatch\ space \times point\ distance}\right)}{layer\ thickness} \tag{1}$$

Three repeats of the cubes were produced for each setting; the array is shown in Fig. 1. All other parameters were maintained at the standard settings as recommended by the machine manufacturer (laser power 180 W, layer thickness 50 µm, 124 µm hatching space and meander path pattern, as shown in Fig. 2).

Table 2 Parameter selection, settings and corresponding laser power (J/mm^3).

		Point Distance (µm)		
		25	50	75
Exposure time (µs)	75	125.42	62.71	41.81
	100	167.23	83.61	55.74
	125	209.03	104.52	69.68

Throughout the build process, the ambient temperature was maintained at 21 ˚C and O$_2$ levels within the chamber were minimised using an argon atmosphere at a maximum 5000 ppm.
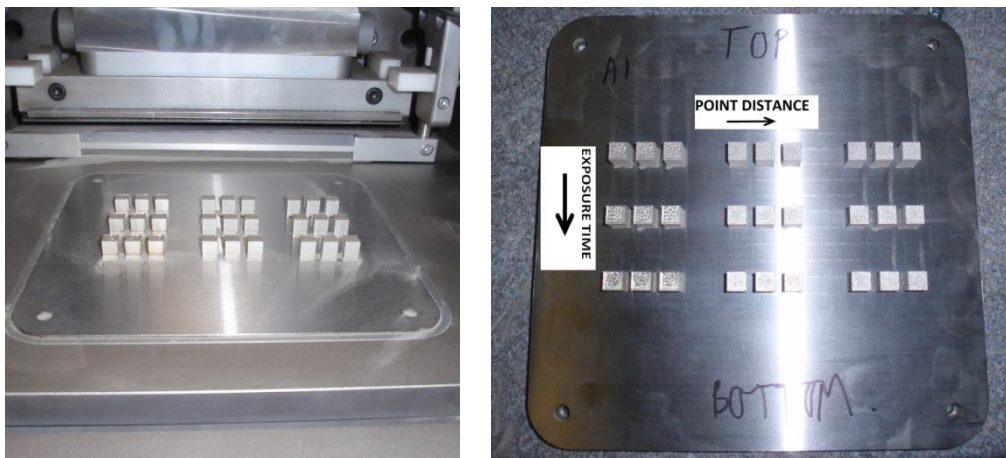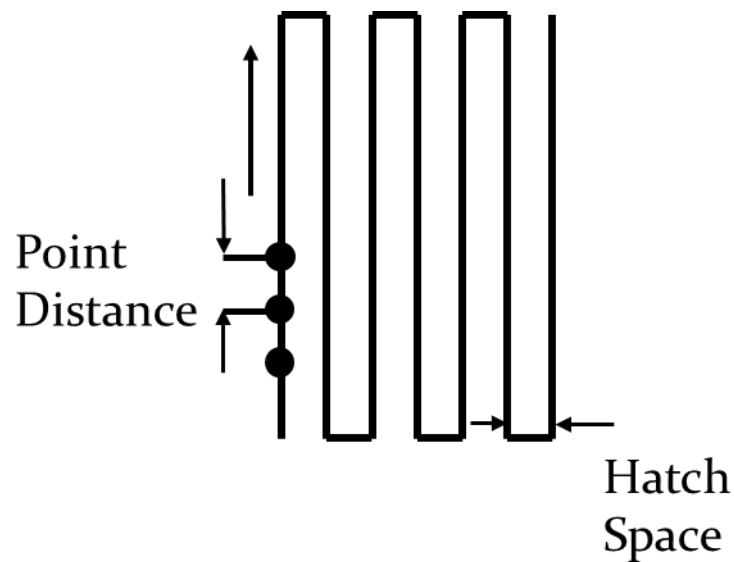

Fig. 1 Layout of Cube array

Fig. 2 Meander path pattern, hatch space and point distance (Arrow displays direction of laser movement)

2.2. Microstructural characterisation and porosity measurements

The cubes were mounted in conductive bakelite and metallographically prepared using standard techniques. Images for each cube were taken using a Reichert MeF3 inverted stage metallographic microscope. Image capture was via Nikon camera DS-Fi1 and Nikon Elements D software. Porosity measurements were taken from the images collected. For each sample, five images were taken at different locations: four at the corners and one at the centre of the cube and these locations are shown in the Fig. 3b.

In-house image analysis software was used to measure the porosity of the cubes. Firstly, the images were converted to black and white using a constant threshold value such that porosity became black and matrix white (Fig. 3a). The ratio of the number of black to white pixels was calculated. Black pixels correspond to porosity and white pixels correspond to matrix.

After the porosity had been measured for each section, the samples were etched using a solution of 100 mL ethanol, 100 mL HCl and 5 g $CuCl_2$. Microstructural analysis was carried out using a JEOL-35C Scanning electron microscope.
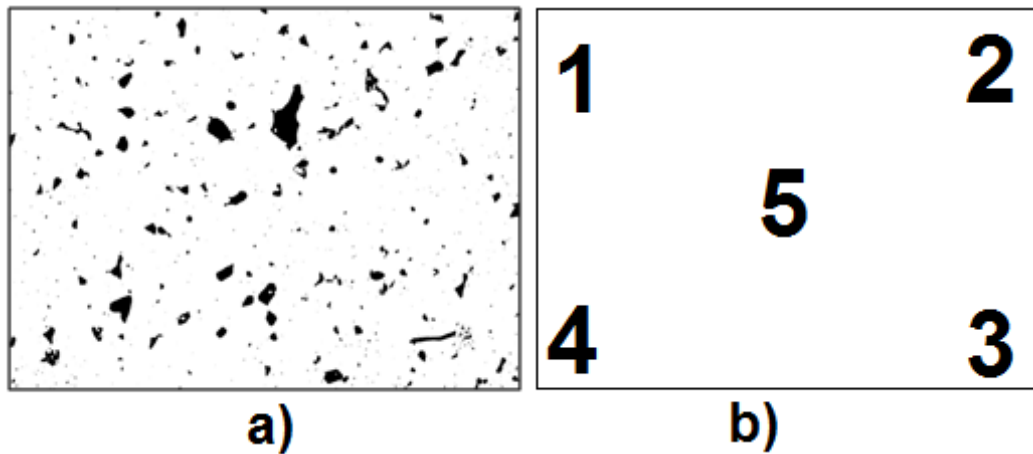
Fig. 3 Porosity measurements on each of the cube samples; a) Porosity and b) Positions on the cubes where images were captured

2.3.   EDX analysis

Energy Dispersive X-ray analysis was carried out on the polished specimens, to determine whether any compositional changes had occurred during the processing/manufacturing operation. On each cube compositional analysis was performed at three random locations using JEOL-35C Scanning electron microscope and Oxford Instrument Aztec EDX software.

2.4.   Hardness

The hardness values were measured at 3 locations per cube and obtained using Vickers indenter on a microhardness machine at a load of 10 kgf.

2.5.   Surface Roughness

The surface roughness (R_a) was measured using the Wyko NT2000 white light interferometer. An average surface roughness was obtained from measurements taken from all four vertical sides of each cube.

3. Results and discussion

3.1.   Composition

EDX analysis revealed that no bulk compositional changes had occurred during the SLM process for the various laser energies used for the builds. An average of 3 recorded values across the whole range of cubes is shown in Table 3, alongside the original composition as quoted by the supplier, measured using EDX analysis on the

sectioned and polished powder. This current finding agrees with the results of Ekrami et al. [13], who conducted a metallographic analysis on 316L stainless steel ALM manufactured parts. They showed that the ALM process does not disintegrate any metallic elements from alloy.

Table 3 EDX analysis of cubes and comparison with supplier's composition

Element	Average recorded value	Supplier composition
	Wt%	Actual
Si	0.8 ± 0.1	0.7
Cr	18.5 ± 0.2	17.9
Mn	1.4 ± 0.1	1.4
Fe	64.0 ± 0.2	64.9
Ni	12.7 ± 0.3	12.7
Mo	2.5 ± 0.2	2.4

Optical micrographs of a polished and etched cube side section are shown in Fig. 4a; the build direction is shown by the white arrow (Fig. 4b). The cross sections of the melted scan tracks are visible as curved "troughs", shown by the black arrows in Fig. 4b, demonstrating that the particles have fused together within the melted and solidified zones. The laser tracks overlap so that each melted track is bonded onto the other tracks. At higher magnification (via SEM), Fig. 5, a fine cellular/dendritic structure is apparent which is characteristic of laser based processing. Yasa and Kruth [14] have observed a similar dendritic microstructure in 316L stainless steel ALM manufactured parts.

Such a structure is produced as a result of rapid solidification due to high cooling rates within the process. Previous work on 316L stainless steel [1] has demonstrated that secondary dendrite arm spacing below 1 µm is a feature characteristic of high strength.
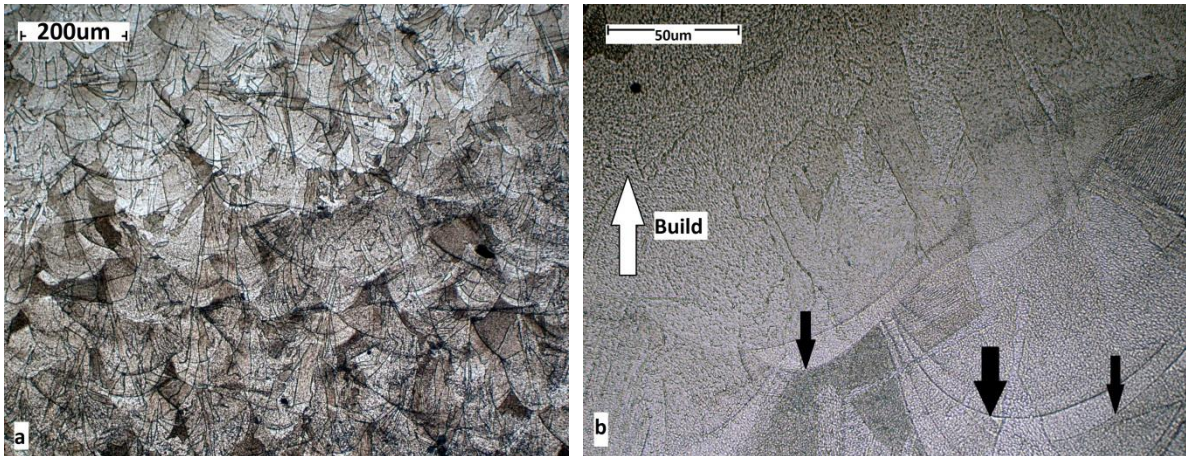
Fig. 4 Optical images of side surface (polished and etched). Build direction shown by white arrows, melted scan tracks shown by black arrows.
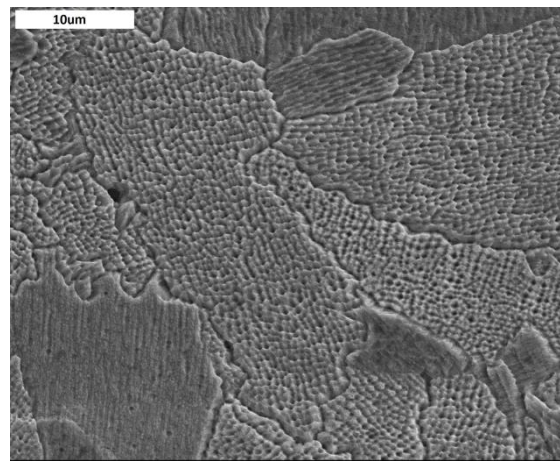

Fig. 5 SEM image of side surface (polished and etched)

3.2. Balling

Balling has been the focus of a number of studies as it is one of the critical process induced defects associated with ALM parts and can result in a poor surface finish of the part. Gu and Shen [15] studied the balling effect in 316L stainless steel in an attempt to eradicate it during the production of ALM parts. Tolchko et al. [16] studied the detailed kinetics of the balling phenomenon for nickel alloy powders. Under unfavourable laser processing parameters (speed, energy etc) they determined that the molten metal breaks into droplets instead of spreading uniformly on the underlying surface. This phenomenon of droplet formation is known as balling and was observed for certain builds in the current study, at various laser energy densities. Balling is primarily governed by the wetting/surface tension characteristic of both the molten powder, solid powder and the solid surface [17] and is strongly influenced by the temperature of both the molten powder particles and solid surface. The temperature will be influenced by the enegry imparted to the material and is directly related to the process parameter variation explored in this paper. Li et al. [18] studied the effect of sulphur contents on surface tension

of molten stainless steel using sessile drop method. The results showed that surface tension is affected by temperature and sulphur contents of stainless steel. However, the levels of sulphur content are extremely low in the 316L material used for this study and detecting variations in in sulphur content in specific areas was not possible.

To highlight the balling phenomenon, the top surface topography of the cubes, manufactured using three different laser energy densities: 41.81 J/mm^3, 104.52 J/mm^3, 209.03 J/mm^3, is shown in the Fig. 6. Surface balling is most apparent at energies of 41.81 J/mm^3, Fig. 6a and 209.03 J/mm^3, Fig. 6c, while a laser energy density of 104.52 J/mm^3 shows the least surface balling, Fig. 6b . The direction of the scan tracks is clearly visible within Fig. 6d and the width of these tracks is measured to be 70-80 μm. The scan tracks have two paths: one going up and down, the other path is slightly inclined and also bi-directional, such a pattern is known as an "alternating bi-directional pattern." Kruth et al. [1] investigated the effect of three different types of scan strategies on density in Ti6Al4V ALM manufactured parts. A maximum of 99.85 % density was reported using alternating bi-directional pattern as the risk of having un-melted regions between the two adjacent tracks is minimized. Their findings support the current porosity results; see Fig. 7, where optimum porosity of 0.38 % was attained at a laser energy density of 104.52 J/mm^3.
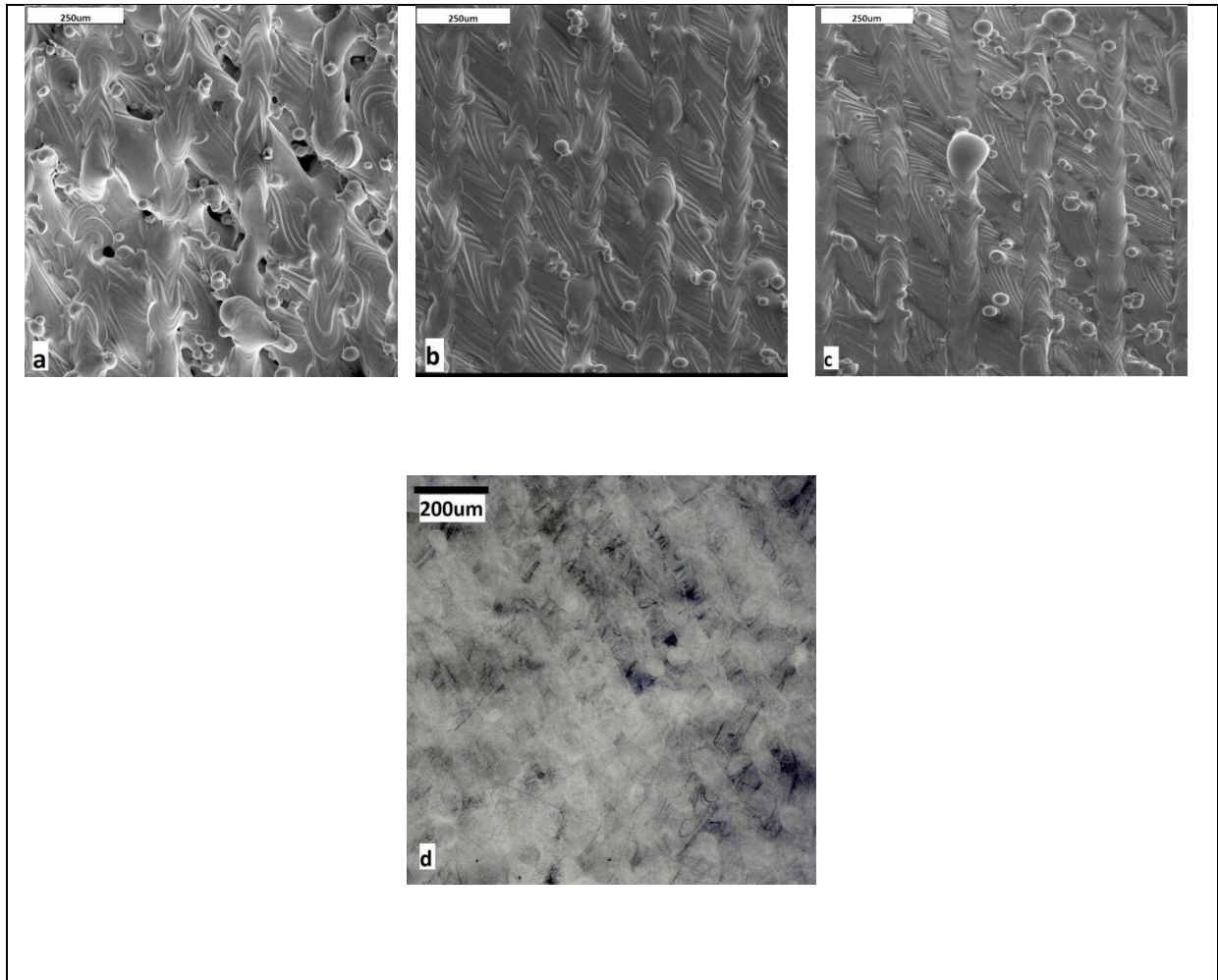
Fig. 6 SEM images showing topography of top surface of builds manufactured using three different laser energy densities: a) 41.81 J/mm^3, b) 104.52 J/mm^3 and c) 209.03 J/mm^3 and d) polished and etched top section at 104.52 J/mm^3

At a low laser energy density (41.81 J/mm^3) scan tracks were discontinuous and gaps were visible in between the tracks. Ellipsoidal and spherical balls of variable size usually smaller than 50 µm were cohered to surface of the tracks and within the gaps (Fig. 6a) resulting in a poor surface finish. At a low laser energy density, the as-formed molten pool temperature and dimensions are small limiting the contact area between the molten pool, metal powder particles and substrate. Li et al [19] showed that incomplete melting combined with unfavourable wetting characteristics at low energy, gives rise to balling. It has been shown that the relative density and randomness of the powder bed as well as the relative size of the melt pool compared to the powder particle diameter also significantly affect balling.

An increase in laser energy density from 41.81 to 104.52 J/mm^3 resulted in merging of the scan tracks and an overall smoothing of the surface. Fewer spherical balls were visible on the surface of scan tracks, Fig. 6b. This higher laser energy density has been shown by Gu and Shen [15] to promote a stable melt pool with favourable

surface tension and wetting characteristics due to an increase in the molten materials temperature resulting in smooth scan tracks free of balling.

At a laser energy density of 209.03 J/mm^3 tracks were continuous but were accompanied by an increase in balling (~100 μm) (Fig. 6c) when compared to that of 104.52 J/mm^3. This could again be attributed to a change in the composition of the molten material and subsequent increase in surface tension due to reduction of sulphur content and further increased temperature [18].

Previous studies by Gu and Shen [15] have shown that a higher laser energy density accompanied by low scan speed creates a melt pool with a long liquid life time and high superheat. This provides enough input energy and time for molten metal to split into droplets as described by Khan and Dickens [20]and their processing on 24 carat gold powder giving rise to the balling phenomena observed in this study.

In summary, the present study has shown a variation in balling effect and supports the work of Li et al. [19] who reported on the effect of laser processing parameters on balling in 316L stainless steel and nickel powders.

3.3. Porosity

Porosity is typically observed in ALM parts and represents the most common defect, the degree of which can be altered via the laser processing parameters. In a previous study, Li et al. [21] has analyzed the effect of laser processing parameters on porosity of ALM parts using 316L stainless steel powder.
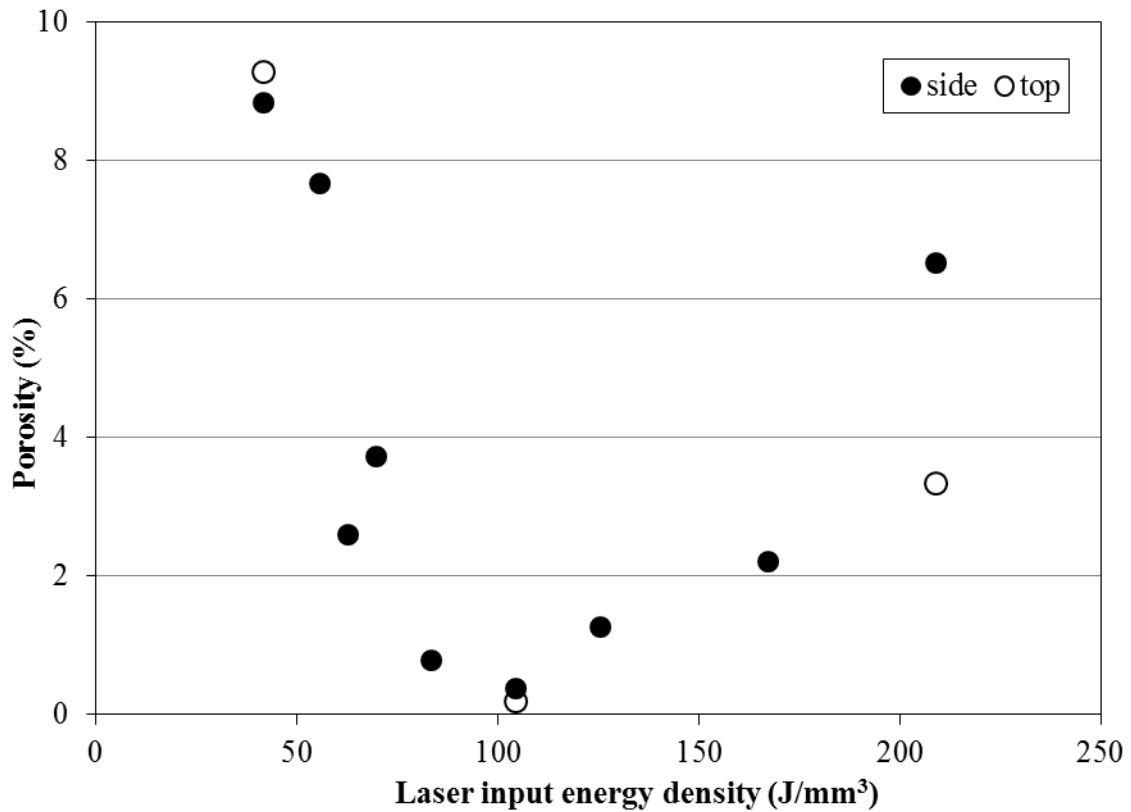
Fig. 7 Porosity versus laser energy density for builds, data points are measured values of porosity from optical microscopic images on one of the sides face (•) and top face (o) of the cubes which is build direction.

The effect of laser input energy density on the porosity was determined for two different sides of the cubes, Fig. 7. Filled circles represent porosity as measured on a side face while hollow circles represent porosity as measured on the top face of the cubes. Similar trends are seen for top and side face porosity, indicating that porosity is distributed uniformly throughout the build.

At a low laser energy density (41.81 J/mm^3) porosity is at a peak (8.84 %). Pores are uniformly dispersed, irregular in shape and interconnected, with a defined orientation along the surface, Fig. 8a-b. The porosity is characterised by large cavities as big as 220 μm filled with loosely held particles of 25 μm, (Fig. 8a). Due to the size of the entrapped particles (5-45 μm), it is likely, that these are un-melted powder particles. A possible explanation for this is that at such a low laser energy density, the size of melt pool is small [3] and powder particles are not molten enough to ensure sufficient bonding between the layers due to lower penetration depth of laser.

Increasing laser energy density from 41.81 J/mm^3 to 104.52 J/mm^3 decreases porosity from 8.84 % to 0.38 %. Simchi [22] studied the effect of laser intensity on the densification of iron based powders, showing that increasing laser energy density, establishes a relatively high temperature that eases liquid flow to fill pores

(voids). This is due to the relatively low viscosity of melt and hence part density increases. Simchi [12] studied the influence of laser processing parameters on densification for various powders such as Fe, Fe–C, Fe–Cu, Fe–C–Cu–P, 316L stainless steel, and M2 high-speed steel. The results showed that density is linearly proportional to ratio of laser power to scan rate.

At higher laser energy densities pores are mostly spherical in shape, Fig. 8c-d, and porosity is localized - the high magnification image, Fig. 9b shows a porosity free area. The presence of such small pores in an ALM microstructure has been reported by Hao et al. [3] to be as a result of gas voids and solidification shrinkage.
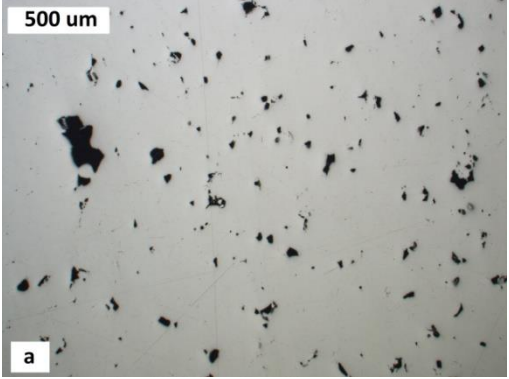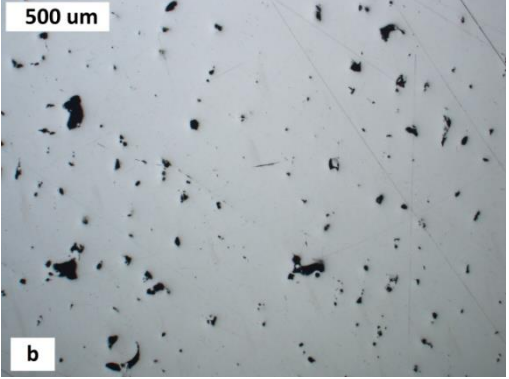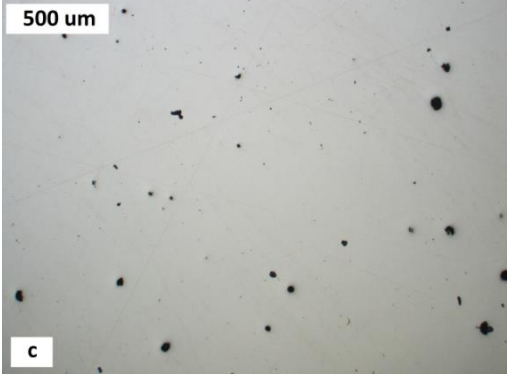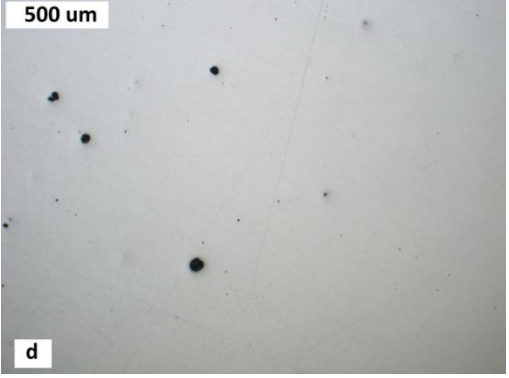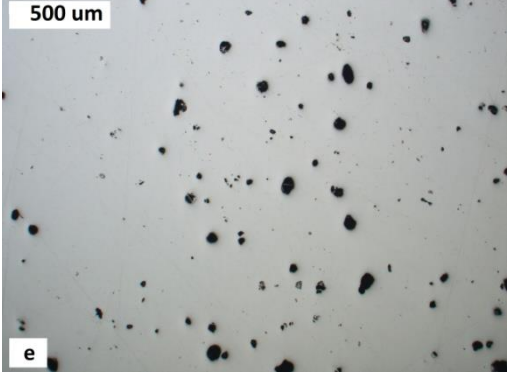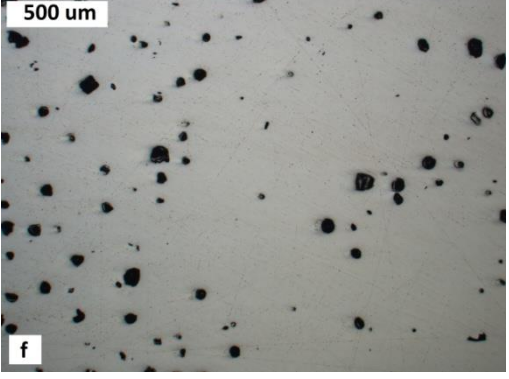
Laser energy density (J/mm^3)	Sides	Tops
41.81	500 um a	500 um b
104.52	500 um c	500 um d
209.03	500 um e	500 um f

Fig. 8 Optical images showing the best and worst examples of porosity.

On raising the laser energy density from 104.52 J/mm^3 to 209.03 J/mm^3, porosity increases from 0.38 % to 6.51% and the pores are seen to increase in size, Fig.8 e-f and Fig. 9c. This higher laser energy density could cause vaporisation of low melting elements, which become entrapped, leaving behind the pores [23]. Further work by Taha et al. [24] highlighted such pores could either be within a built layer or between two layers. Observation by Kruth et al. [1] have been made for 316L stainless steel parts where decreasing scan speed

results in formation of bigger grain size and irregular melt pool, which deteriorates part quality by the formation of large pores. Work by Campanelli et al. [23] has also suggested that the presence of a small amount of oxygen (0.02 wt %) and carbon (0.02 wt %) in 316L stainless steel could react at high temperature to form gaseous products such as CO or CO_2 - which could produce spherical pores in the build due to gaseous entrapment. Any moisture or contaminants such as oxides present on the surface of powder particles, as suggested by Taha et al. [24], are also source of gaseous porosity and localized delamination or debonding. Larger melt pools formed at higher laser energies may also be more susceptible to solidification micro shrinkage porosity.

A variation in porosity where it first decreases by increasing laser energy density and then increases by further increments in laser energy density has also been seen by Zhang et al. [25] for Mg powders.
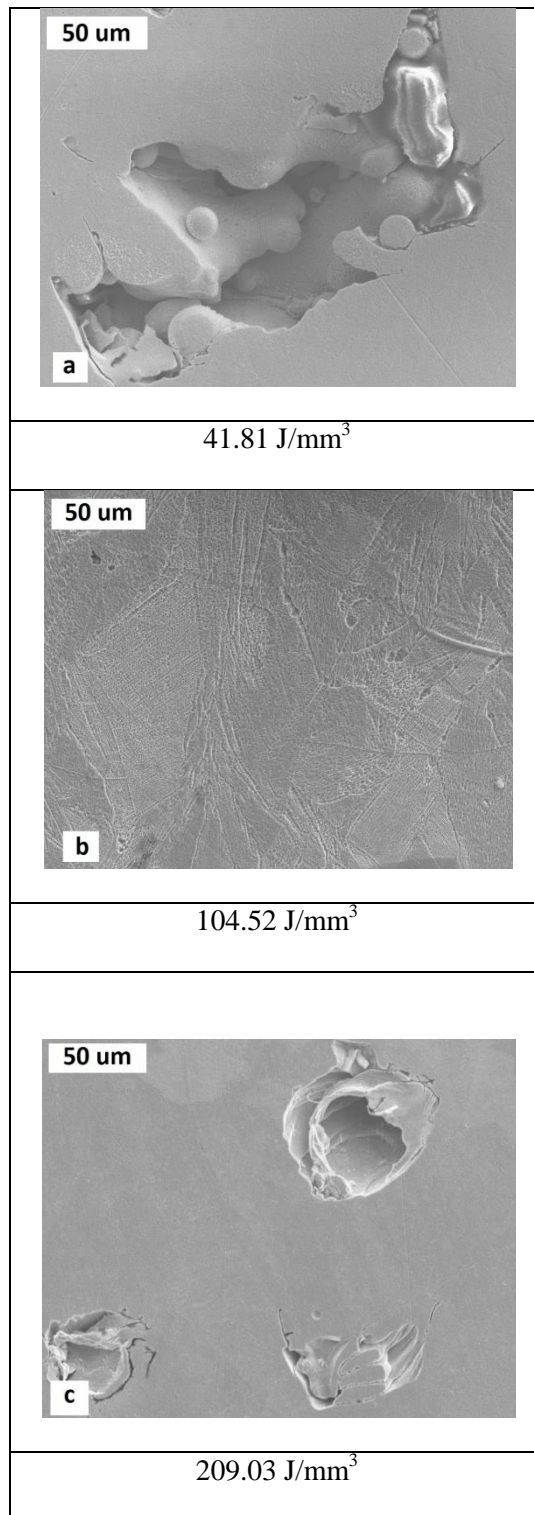
50 um

a

41.81 J/mm^3

50 um

b

104.52 J/mm^3

50 um

c

209.03 J/mm^3

Fig. 9 SEM images of polished surfaces to show internal porosity.

3.4. Hardness

The indent size created at the highest porosity is displayed in Fig. 10. The indent is larger than the pores at the lowest porosity, although overlap is observed. The overlap of indent with the pores is necessary to obtain a true representation of the material hardness due to variations in porosity, rather than variations in the fully dense material. The hardness of the fully dense material could be affected by the differences in energy imparted during the SLM process and subsequent variations in temperature and heating/cooling rates. The change in hardness due to the variation in porosity is of greater importance when considering a manufactured component.

The material hardness is shown to increase with energy until a maximum of 225 HV at 125 J/mm^3 which is typical of hardness achieved using SLM as specified by Tolosa et al. [26] where mean values of 235 HV are obtained, Fig. 11. Further increases in energy display a reduction in material hardness. The hardness results show a general relationship to the results displayed for the porosity of the material with varying energy input, Fig. 12. As porosity increases, hardness decreases. This is primarily due to the pores within the material collapsing under load. Further hardness variations could also be attributed to the energy and subsequent temperature the laser has imparted to the material causing variations in heating/cooling rates. It is clear that by optimising the laser energy input the porosity (i.e. density) of the material and its as-manufactured hardness can be controlled.
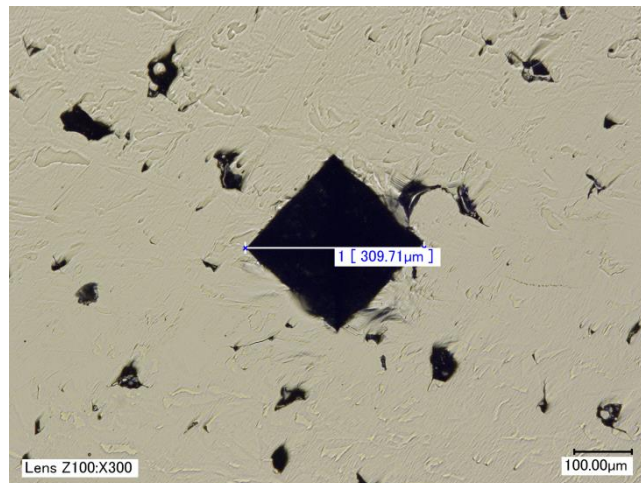

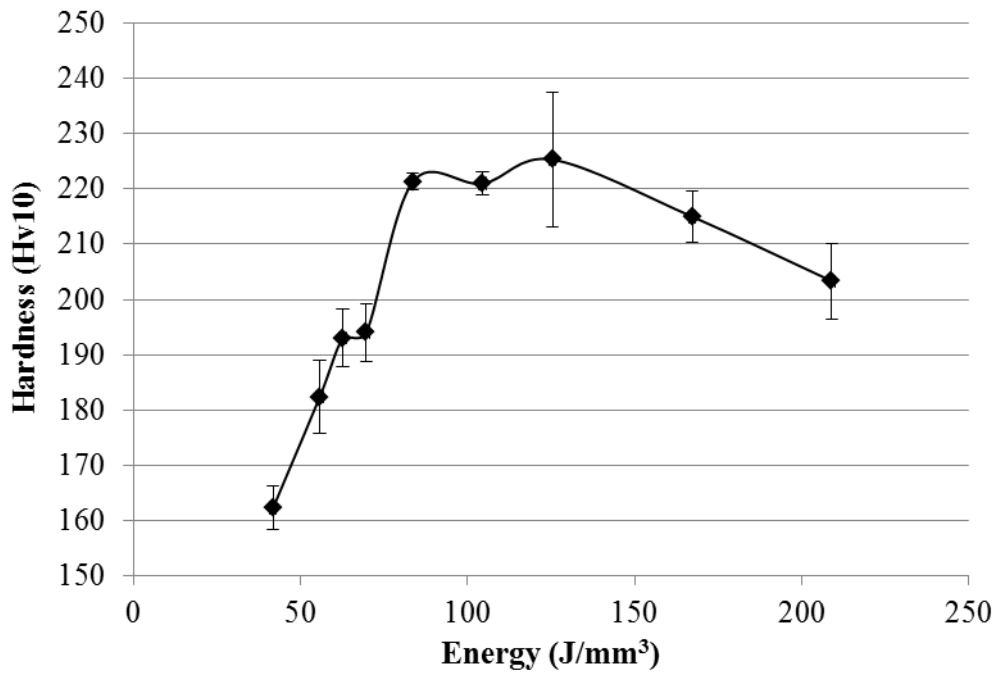**Fig. 10** Hardness Indent at 41.81J/mm^3
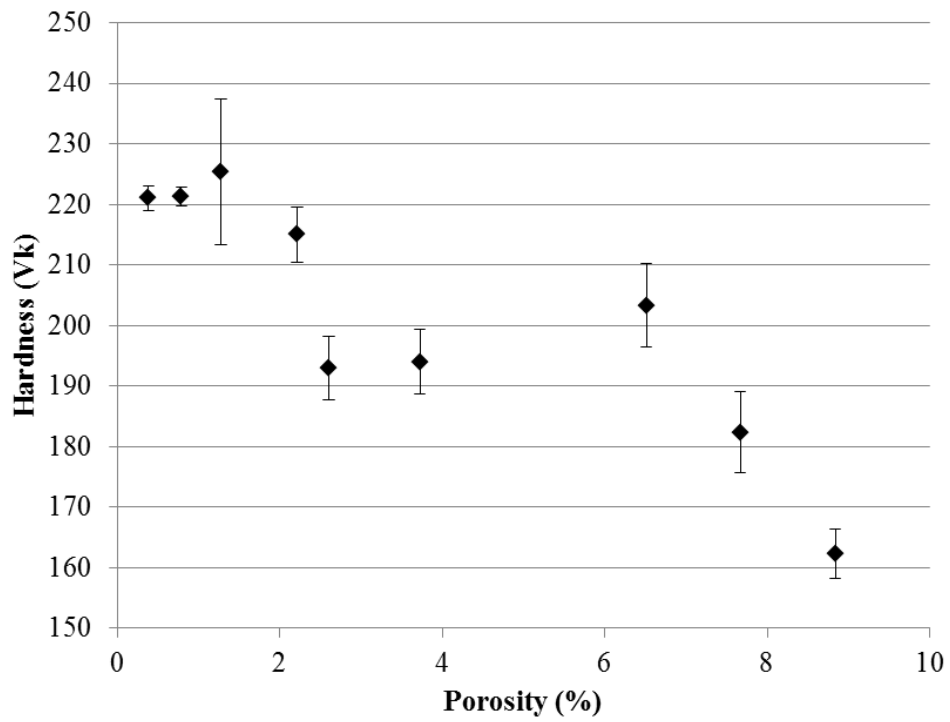
Fig. 11 Hardness versus Laser Energy

Fig. 12 Hardness versus percentage porosity

3.5. Surface Roughness

The effect of energy, exposure time and point distance have been used to determine the effect on surface roughness, Figs. 13, 14 and 15. This enables each method of changing the energy input to be assessed independently. As previously seen with the porosity, the surface roughness follows the same trend, where a reduction in surface roughness is observed with increased energy until an optimum level is obtained, when further increases are detrimental to the surface finish. The optimal surface finish and porosity are not observed at the same energy input, indicating a compromise between surface finish and porosity. The lowest surface roughness was measured at an energy input of 125.4 J/mm^3, obtained at a 25μm point distance and 75μs exposure time. The highest surface roughness was obtained at 69.6 J/mm^3, obtained at a 75μm point distance and 125μs exposure time. This indicates the requirement to assess surface finish by the each method of varying energy input.

Exposure time has minimal effect on the surface roughness, with R_a values between 9 and 16 μm depending on point distance. Taking into account the errors displays no underlying trends can be concluded with certainty.

Point distance displays a trend of increased surface roughness with R_a increasing from approximately 10μm to 15μm with increasing point distance from 25 μm to 75 μm. This is attributed to the reduction in laser overlap due to the increased point distance creating the rougher surface finish, Fig. 16.
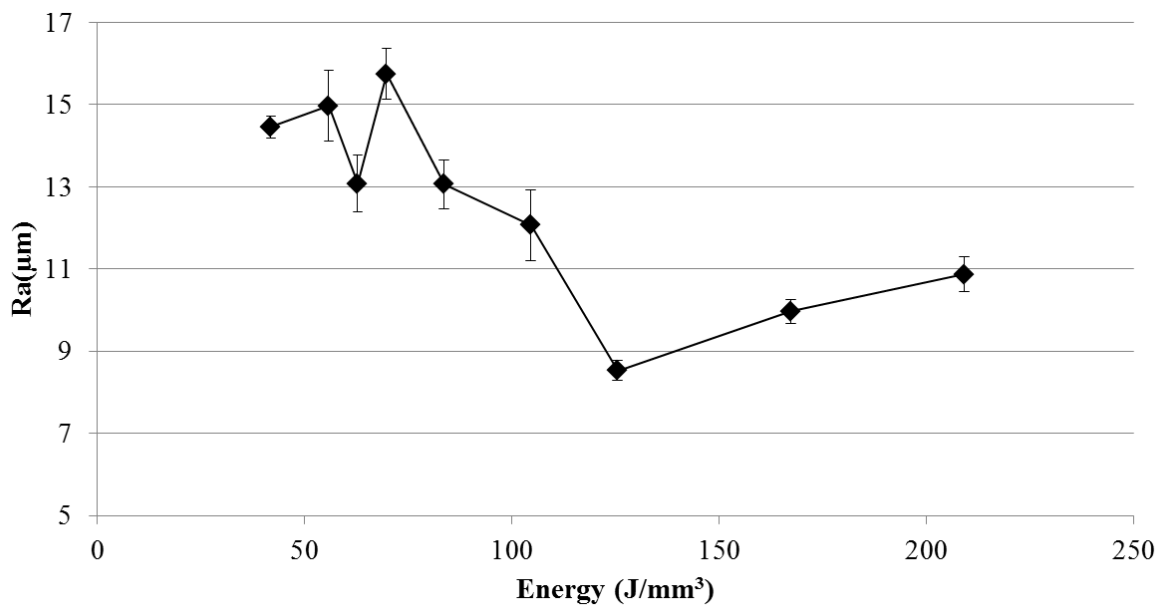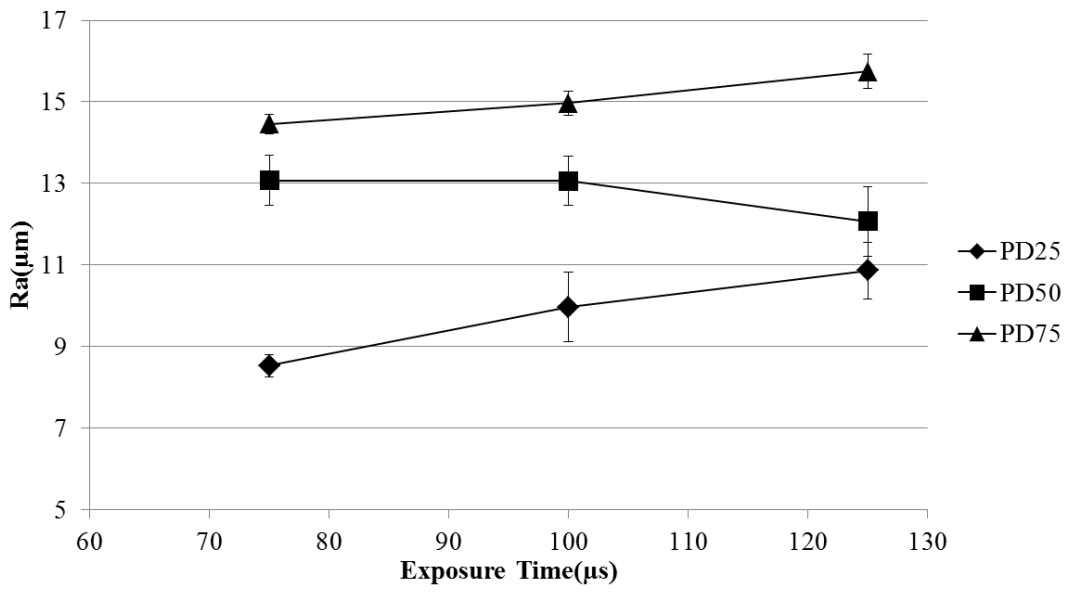
Fig. 13 The effect of energy on surface roughness

Fig. 14 The effect of exposure time on surface roughness
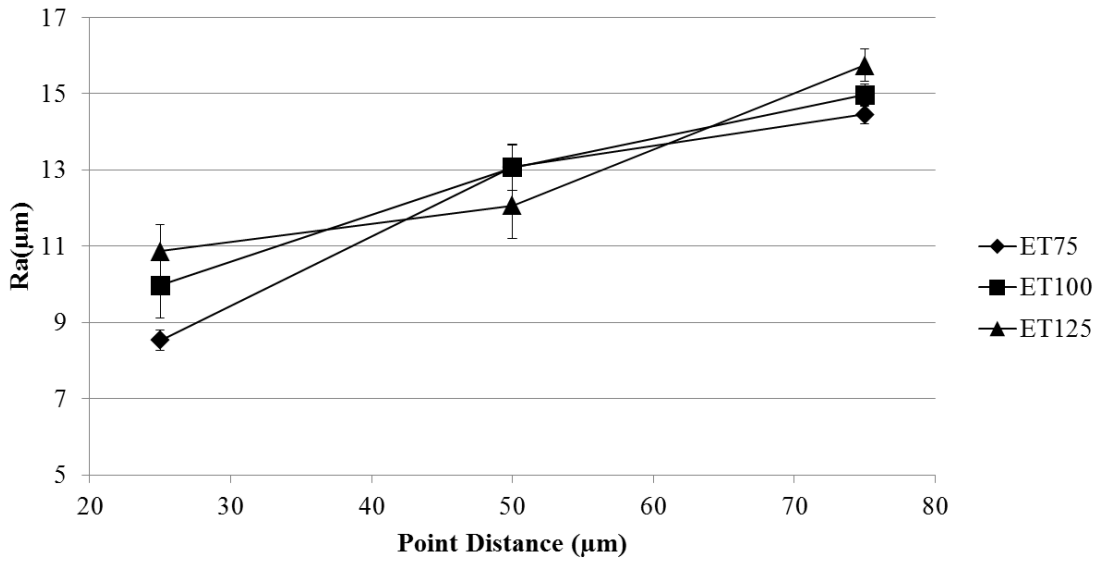

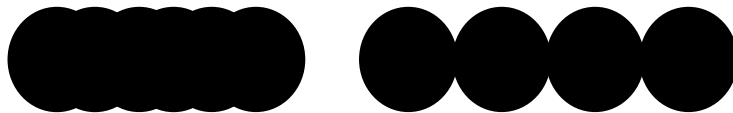**Fig. 15** The effect of point distance on surface roughness

Fig. 16 Schematic of point distance on surface roughness.

4. Conclusions

In this study the effect of processing parameters on microstructure and porosity was studied for the cubes manufactured using the ALM process from 316L stainless steel powder. A systematic characterization of porosity and microstructure shows a number of findings which are summarized as follows:

- o Surface balling is most apparent at both low and high laser energy densities. An optimum surface topography with continuous line tracks and minimum balling was achieved at 104.52 J/mm^3

- o Variations in surface balling appearances were observed; with small-balls dominating at low laser energy density to a mixture of both small and large ball features at high laser energy density.

- o Total porosity is found to be a strong function of laser energy density. At low laser energy porosity is highest; this decreases as laser energy density increases, only to increase again with further increases in the laser energy density. The minimum amount of porosity was observed at 104.52 J/mm^3.

- o Material Hardness increases with decreased porosity to a maximum of 225 HV.

- o The point distance was seen to have a larger effect on surface roughness than the exposure time. Increases in point distance led to increased surface roughness.

- o Altering the laser energy density can result in the production of dense parts. Cubes with density of 99.62 % were produced using laser energy density of 104.52 J/mm^3 and this is seen to be the optimum laser energy density during the current investigation.

Acknowledgements

References

[1] Kruth J P, Badrossamay M, Yasa E, Deckers J, Thijs L and Humbeeck J V, "Part and material properties in selective laser melting of metals," in 16th International symposium on electromachining (ISEM XVI), 2010, DOI: https://lirias.kuleuven.be/handle/123456789/265815

[2] Paul B K and Baskaran S, "Issues in fabricating manufacturing tooling using powder-based additive freeform fabrication," Journal of materials processing technology, vol. 61, pp. 168-172, 1996, DOI: http://dx.doi.org/10.1016/0924-0136(96)02482-X

[3] Hao L, Dadbakhsh S, Seaman O and Felstead M, "Selective laser melting of a stainless steel and hydroxyapatite composite for load-bearing implant development," Journal of materials processing technology, vol. 209, pp. 5793-5801, 2009, DOI: http://dx.doi.org/10.1016/j.jmatprotec.2009.06.012

[4] Mathisen M B, "In-Situ Tensile Testing Combined with EBSD Analysis of Ti-6Al-4V Samples from Components Fabricated by Additive Layer Manufacture," Materials Science and Engineering, Submitted June 2012, DOI: http://www.diva-portal.org/smash/record.jsf?pid=diva2:566362

[5] Su X and Yang Y, "Research on track overlapping during selective laser melting of powders," Journal of materials processing technology, vol. 212, pp. 2074-2079, 2012, DOI: http://dx.doi.org/10.1016/j.jmatprotec.2012.05.012

[6] Gebhardt A, Schmidt F M, Hotter J S, Sokalla W and Sokalla P, "Additive Manufacturing by selective laser melting the realizer desktop machine and its application for the dental industry," in Laser Assisted Net Shape Engineering 6, Proceedings of the LANE 2010, Part 2, 2010, DOI: http://dx.doi.org/10.1016/j.phpro.2010.08.082

[7] Chatterjee A N, Kumar S, Saha P, Mishra P K and Choudhury A R, "An experimental design approach to selective laser sintering of low carbon steel," Journal of materials processing technology, vol. 136, pp. 151-157, 2003, DOI: http://dx.doi.org/10.1016/S0924-0136(03)00132-8

[8] Kruth J P, Froyen L, Vaerenbergh J V, Mercelis P, Rombouts M and Lauwers B, "Selective laser melting of iron-based powders," Journal of materials processing technology, vol. 149, pp. 616-622, 2004, DOI:

http://dx.doi.org/10.1016/j.jmatprotec.2003.11.051

[9] Wang Z, Guan K, Gao M, Li X, Chen X and Zeng X, "The microstructure and mechanical properties of deposited-IN718 by selective," Journal of Alloys and Compounds, vol. 513, p. 518– 523, 2012, DOI: http://dx.doi.org/10.1016/j.jallcom.2011.10.107

[10] Mumtaz K A, Erasenthiran P and Hopkinson N, "High density selective laser melting of Waspaloy," Journal of materials processing technology, vol. 195, pp. 77-87, 2008, DOI: http://dx.doi.org/10.1016/j.jmatprotec.2007.04.117

[11] Liu F, Lin X, Huang C, Song M, Yang G, Chen J and Huang W, "The effect of laser scanning path on microstructures and mechanical properties of laser solid formed nickel-base superalloy Inconel 718," Journal of Alloys and Compounds, vol. 509, no. 13, p. 4505–4509, 2011, DOI: http://dx.doi.org/10.1016/j.jallcom.2010.11.176

[12] Simchi A, "Direct laser sintering of metal powders Mechanism, kinetics and microstructural features," Materials science and engineering A, vol. 428, pp. 148-158, 2006, DOI: http://dx.doi.org/10.1016/j.msea.2006.04.117

[13] Ekrami Y, Forth S C and Waid M C, "Characterization of Electron Beam Free-Form Fabricated 2219 Aluminum and 316 Stainless Steel", Technical Report, NASA, USRP, DOI: http://ntrs.nasa.gov/search.jsp?R=20110008207

[14] Yasa E and Kruth J P, "Microstructural investigation of Selective Laser Melting 316L stainless steel parts exposed to laser re-melting," Procedia engineering, vol. 19, pp. 389-395, 2011, DOI: http://dx.doi.org/10.1016/j.proeng.2011.11.130

[15] Gu D and Shen Y, "Balling phenomenon in direct laser sintering of stainless steel powder: metallurgical mechanisms and control methods," Materials and design, vol. 30, pp. 2903-2910, 2009, DOI: http://dx.doi.org/10.1016/j.matdes.2009.01.013

[16] Tolchko N K, Mozzharov S E, Yadroitsev I A, Laoui T, Froyen L, Titov V I and Ignatiev M B, "Balling process during selective laser treatment of powders," Rapid prototyping journal, vol. 10, no. 2, pp. 78-87, 2004, DOI: http://dx.doi.org/10.1108/13552540410526953

[17] Körner C, Attar E and Heinl P, "Mesoscopic simulation of selective beam melting processes," Journal of Materials Processing Technology, vol. 211, no. 6, p. 978–987, 2011, DOI: http://dx.doi.org/10.1016/j.jmatprotec.2010.12.016

[18] Li Z, Mukai K, Zeze M and Mills K C, "Determination of the surface tension of liquid stainless steel," Journal of materials science, vol. 40, pp. 2191-2195, 2005, DOI: http://dx.doi.org/10.1007/s10853-005-1931-x

[19] Li R, Liu J, Shi Y, Wang L and Jiang W, "Balling behavior of stainless steel and nickel powder during selective laser melting process," Int J Adv Manuf Technol, vol. 59, pp. 1025-1035, 2012, DOI: http://dx.doi.org/10.1007/s00170-011-3566-1

[20] Khan M and Dickens P, "Selective laser melting (SLM) of pure gold," Gold bulletin, vol. 43, no. 2, pp. 114-121, 2010, DOI: http://dx.doi.org/10.1007/BF03214976

[21] Li R, Shi Y, Wang Z, Wang L, Liu J and Jiang W, "Densification behavior of gas and water atomized 316L stainless steel powder during selective laser melting," Applied surface science, vol. 256, pp. 4350-4356, 2010., DOI: http://dx.doi.org/10.1016/j.apsusc.2010.02.030

[22] Simchi A, "Effect of C and Cu addition on the densification and microstructure of iron powder in direct laser sintering process," Materials Letters, vol. 62, pp. 2840-2843, 2008, DOI: http://dx.doi.org/10.1016/j.matlet.2008.01.113

[23] Campanelli S L, Contuzzi N, Angelastro A and Ludovico A D, Capabilities and Performances of the Selective Laser Melting Process, New Trends in Technologies: Devices, Computer, Communication and Industrial Systems, M. J. Er, Ed., Open Access Book, 2010, DOI: http://www.intechopen.com/books/howtoreference/new-trends-in-technologies--devices--computer--communication-and-industrial-systems/capabilities-and-performances-of-the-selective-laser-melting-process

[24] Taha M A, Yousef A F, Gany K A and Sabour H A, "On selective laser melting of ultra high carbon steel: effect of scan speed and post heat treatment," Mat wiss u werkstofftech, vol. 43, no. 11, pp. 913-923, 2012, DOI: http://dx.doi.org/10.1002/mawe.201200030

[25] Zhang B and Coddet C, "Effects of processing parameters on properties of selective laser melting Mg–9%Al powder mixture," Materials and design, vol. 34, pp. 753-758, 2012, DOI: http://dx.doi.org/10.1016/j.matdes.2011.06.061

[26] Tolosa I, Garciandia F, Zapirain F, Zubiri F and Esnaola A, "Study of mechanical properties of AISI 316 stainless steel processed by "selective laser melting", following different manufacturing strategies," *Int J Adv Manuf Technol,* vol. 51, pp. 639-647, 2010, DOI: http://dx.doi.org/10.1007/s00170-010-2631-5